

The Key Role of Lower-Level Meridional Shear in Baroclinic Wave Life Cycles

DENNIS L. HARTMANN

Department of Atmospheric Sciences, University of Washington, Seattle, Washington

(Manuscript received 18 December 1998, in final form 23 March 1999)

ABSTRACT

A series of idealized nonlinear life cycle experiments is performed to compare changes in life cycle behavior caused by upper-level and near-surface meridional shear of the initial zonal wind. It is shown that both the eddy kinetic energy and the zonal flow accelerations produced during a cycle of growth and equilibration respond primarily to the meridional shear of the zonal wind near the surface and only weakly to shear near the tropopause. Near the critical shear for transition from anticyclonic to cyclonic life cycle behavior, the zonal flow accelerations are minimized and the eddy persistence is maximized. Above this critical shear, eddy breaking on the poleward side of the jet increases and strong cyclonic zonal wind shears are generated. The influence of baroclinic shears is minimized by using dipolar wind anomalies that are zero near the center of a basic baroclinic jet and by taking advantage of the fact that the life cycle response is very sensitive to small changes in the magnitude of initial meridional shear. The small baroclinic shears contribute to the differences in the sense that a cyclonic shear decreasing with height is slightly more effective in inducing cyclonic behavior than is a barotropic cyclonic shear with the same surface value. Upper-tropospheric eddy momentum fluxes by linear normal modes are also much more sensitive to lower-tropospheric meridional shear than to upper-tropospheric meridional shear. The primary response of normal modes to lower-tropospheric meridional shear is to change the momentum flux at all levels.

1. Introduction

Idealized numerical experiments simulating the life cycle of midlatitude baroclinic waves have been used to better understand the dynamical and climatological importance of midlatitude eddies. Early experiments of this nature have shown that nonlinear life cycles can explain features of the role of eddies in the general circulation that linear normal-mode theory cannot (e.g., Gall 1976; Simmons and Hoskins 1978). Nonlinear life cycle experiments show that strong eddy momentum fluxes and zonal flow accelerations are produced in the late stages of baroclinic wave life cycles when eddy energy is converted to zonal kinetic energy. Under normal conditions on the sphere, the eddy kinetic energy decays nearly as fast by barotropic processes as it grows by baroclinic processes, and this usually results in a narrowing and poleward displacement of the westerly winds. Recent investigations with primitive equation models have traced this tendency for poleward jet movement to the metric effect of the convergence of meridians (Whitaker and Snyder 1993; Balasubramanian and Garner 1997).

An important subtheme of baroclinic life cycle experiments has been the study of the role of meridional shear

of the barotropic component of wind. Simmons and Hoskins (1980, hereafter SH) studied the effect of a wide range of barotropic wind anomalies on baroclinic jets. They found that adding westerly barotropic wind at the latitude of a westerly baroclinic jet reduces the maximum kinetic energy achieved, and adding easterly wind increases it. The role of meridional shear in limiting baroclinic energy release has been called the barotropic governor effect (e.g., James 1987; Nakamura 1993). In addition, cyclonic shear across the jet increases the eddy kinetic energy attained during a life cycle, while anticyclonic shear reduces it. Cyclonic shear can be imposed by simultaneously placing westerlies equatorward of the baroclinic jet and easterlies poleward of it, in which case we can speak of a zonal wind anomaly with "rotation" about the jet axis. In cases with such barotropic-shear anomalies with rotation, an interesting life cycle behavior can be obtained in which the kinetic energy attains a relatively large value but does not decline rapidly by barotropic energy conversions and so retains high eddy energy for an extended period (SH). The structures of these long-lived eddies are characterized by stable, large-amplitude undular waves (Thorncroft et al. 1993, hereafter THM). Many investigations have used the baroclinic wave life cycle approach to investigate the development of surface features and their relation to shear, surface drag, and other effects (e.g., Thorncroft and Hoskins 1990; Davies et al. 1991; Rotunno et al. 1998; Wernli et al. 1998) as well as upper-level features (e.g., Heckley and Hoskins 1982; Bush and Peltier 1994).

Corresponding author address: Prof. Dennis L. Hartmann, Department of Atmospheric Sciences, Box 351640, University of Washington, Seattle, WA 98195.
E-mail: dennis@atmos.washington.edu

Recently Hartmann and Zuercher (1998, hereafter HZ) have shown that the transition of life cycle behavior from anticyclonic wave breakdown to a long-lived cyclonic eddy takes place over a very narrow range of the barotropic shear parameter, corresponding to initial differences of the zonal flow of less than 1 m s^{-1} . A simple interpretation of the growth, upward propagation, saturation, and equatorward breaking paradigm of baroclinic wave life cycles (Gall 1976; Simmons and Hoskins 1978; Edmon et al. 1980) suggests that eddy transports at upper levels play a critical role in the transition from anticyclonic to cyclonic life cycle behavior. Diagnostic studies show a strong signature of upper-level eddy momentum transports in the anticyclonic cases that does not appear in the cyclonic cases (THM, HZ). Recent work by Whitaker and Snyder (1993) and Balasubramanian and Garner (1997) suggests that low-level flow and near-surface kinematics, rather than upper-level wave propagation processes, are critical in the transition. Surface boundary conditions are known to be critical in the development of baroclinic instability and eddy life cycle evolution (e.g., Bretherton 1966). Analysis of highly disturbed flows using tangent linear models suggests that rapidly growing disturbances originate in the lower troposphere near where the wind speed and eddy phase speed are similar (e.g., Buizza and Palmer 1995; Hartmann et al. 1995). Therefore, much intuitive and experimental evidence suggests that low-level flow is critical in baroclinic eddy development.

This work seeks to answer the question of whether the transition from anticyclonic to cyclonic life cycle behavior is more sensitive to near-surface or near-tropopause zonal wind anomalies. The sharp transition from anticyclonic to cyclonic life cycle behavior enables a set of numerical experiments in which the role of lower-level versus upper-level meridional shear can be investigated while minimizing the effect of the baroclinic-shear anomalies that are necessarily involved with such an experiment. The results show clearly that it is initial shear near the surface rather than shear near the tropopause that is critical in determining flow evolution in nonlinear baroclinic life cycle experiments. Baroclinic shears are also important, but they appear to play a lesser role in these experiments.

2. Model and experimental design

We use a spherical primitive equation model with T63 horizontal resolution and 20 vertical levels, much as in

HZ. We have conducted most of the critical experiments with both the model described in Yu and Hartmann (1993), which has a finite element representation in the vertical, and with a model that has simple centered finite differences in the vertical and is described in Held and Suarez (1994). Virtually identical results are obtained with these two models when run at T63L20 resolution. All of the experiments are done without surface drag or heating and with the only subgrid physics being a ∇^6 diffusion of vorticity, divergence, and temperature, with a coefficient set so that the highest resolved wavenumber is damped with a timescale of 2.4 h.

The basic life cycle experiment is conducted by starting with a balanced zonal flow with a basic baroclinic 45° jet as in THM and HZ, to which a small wavenumber-6 perturbation is added. From this a normal-mode instability grows to finite amplitude and interacts strongly with the zonal flow. To the basic 45° jet structure, we add a Gaussian perturbation that has a westerly wind anomaly at 30° and an easterly wind anomaly at 60° , each with an amplitude of U_0 , as in (1):

$$u_s(\phi) = U_0 \left\{ \exp\left(-\left(\frac{\phi - 30^\circ}{12.5^\circ}\right)^2\right) - \exp\left(-\left(\frac{\phi - 60^\circ}{12.5^\circ}\right)^2\right) \right\}. \quad (1)$$

The latitudes (ϕ) of the maximum anomalies have been moved from 20° and 50° —as in earlier studies of SH, THM, and HZ—to 30° and 60° so that the anomaly at the center of the baroclinic jet is zero. This is intended to minimize the effect of baroclinic-shear anomalies on the growth rate.

In addition to the meridional structure of the wind anomaly, we also specify three possible vertical structures for this wind anomaly. The first is a purely barotropic structure as in earlier work, in which the shear anomaly is independent of pressure, and it is denoted by the prefix B for barotropic. The second is a vertical structure that peaks at the surface and goes to zero at $\sigma \leq 0.3$, and it is denoted by the prefix L for lower. The third is a structure that is 1.0 at $\sigma \leq 0.3$, goes to zero at the surface, and is denoted by U for upper. The structure of the transitions is given by a half-cosine wave with a half-power point at $\sigma = 0.65$. The formulas for the vertical structure functions are given in (2), where $\sigma = p/p_s$ is the vertical sigma coordinate, and the vertical structures are plotted in Fig. 1:

$$A(\sigma) = \begin{cases} 1.0 & \text{for } 0.0 \leq \sigma \leq 1.0: & \text{B = barotropic shear} \\ \frac{1}{2} \left(1 + \cos \pi \left(\frac{1 - \sigma}{1 - 0.3} \right) \right) & \text{for } 0.3 < \sigma \leq 1.0; \text{ else } 0.0: & \text{L = lower shear} \\ \frac{1}{2} \left(1 - \cos \pi \left(\frac{1 - \sigma}{1 - 0.3} \right) \right) & \text{for } 0.3 < \sigma \leq 1.0; \text{ else } 1.0: & \text{U = upper shear.} \end{cases} \quad (2)$$

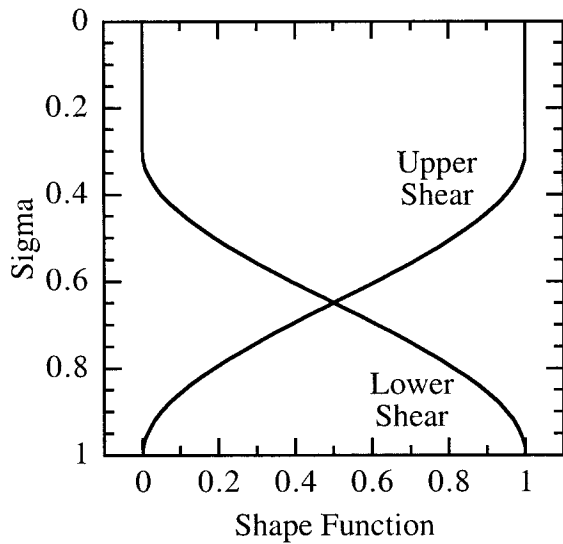


FIG. 1. Vertical structures of zonal wind anomalies for upper-shear case (U) and lower-shear case (L) as functions of sigma.

The basic 45° jet is modified by adding an anomaly given by

$$u'(\phi, \sigma) = u_s(\phi)A(\sigma). \quad (3)$$

Using (1)–(3) we can define a nomenclature for various anomaly configurations, where we construct the anomalies as a product of the horizontal and vertical structure functions. For example, B10 denotes a barotropic-shear anomaly with a magnitude corresponding to $U_0 = 10 \text{ m s}^{-1}$, L8 denotes a lower-shear anomaly with $U_0 = 8 \text{ m s}^{-1}$, and so forth. In addition, we will find it useful to consider hybrid anomalies, which we can denote, for example, with B6 + L2, which indicates a barotropic-shear anomaly of 6 m s^{-1} plus a lower-shear anomaly of 2 m s^{-1} . The structure of a lower-shear anomaly with a magnitude of 2 m s^{-1} is shown in Fig. 2. Such hybrid anomalies are useful in minimizing the effects of baroclinic shear in the investigation of the relative importance of upper and lower meridional shear anomalies. Examples of initial states B0, B8, U8, and L8 are shown in Fig. 3. Of course B0 is just the basic 45° jet without an anomaly. One notices immediately that when the zonal wind anomalies are applied near the surface they are a much larger percentage of the basic jet flow than at upper levels, since the surface winds are constrained to be zero in the basic jet. Experiments to be presented here will show just how important the low-level wind changes are for the life cycle energetics and the structure of the zonal flow accelerations produced at all levels.

3. Life cycle energetics

Although we have used different latitudes for the centers of the westerly and easterly wind anomalies than HZ, we see a similar sharp transition from anticyclonic

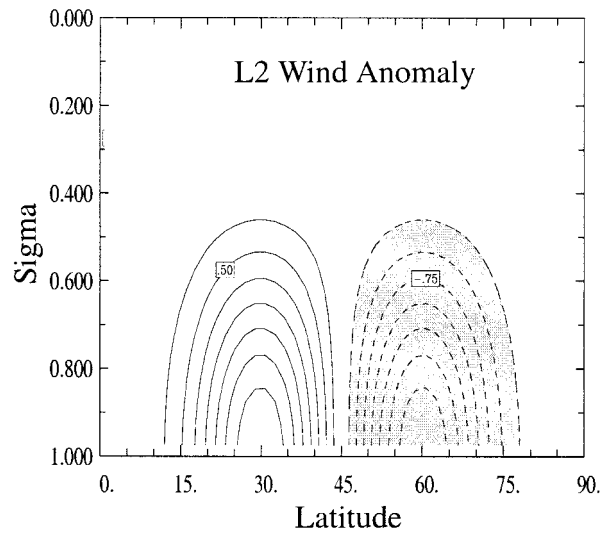


FIG. 2. Latitude vs sigma cross section of L2 anomaly. Contour interval is 0.25 m s^{-1} ; negative contours are shaded.

to cyclonic life cycle behavior as the shear parameter U_0 is increased. Between case B6 ($U_0 = 6 \text{ m s}^{-1}$) and case B8 ($U_0 = 8 \text{ m s}^{-1}$) the barotropic conversion that causes eddy kinetic energy to decline rapidly disappears, and the zonal flow accelerations produced by the wave life cycle change significantly. This transition also occurs when the shear is applied only in the lower part of the troposphere but does not occur if the shear is only applied in the upper part of the troposphere. The response to large-shear anomalies with different vertical structures will be considered first. Figure 4 shows the temporal evolution over a 20-day integration of the eddy kinetic energy in cases B0, B10, U10, and L10. Eddy structures that maintain their kinetic energy at high levels for long periods are achieved in the barotropic-shear (B10) and lower-shear (L10) cases but not when the shear is confined to the upper layer (U10). A life cycle experiment with the magnitude of the upper-level shear anomaly increased to 16 m s^{-1} (U16) still gives an anticyclonic eddy life cycle, so it is not simply that upper-level shears require a larger magnitude to cross a threshold to cyclonic behavior. Such large upper-level shears move the baroclinic zone equatorward, and this may encourage anticyclonic behavior, so that large upper-level shears tend to have a counterbalancing baroclinic effect. Evidence will be presented later that the life cycle behavior is sensitive to rather small meridional-shear changes at low levels.

The eddy kinetic energy evolution of L10 is significantly different from that of B10 (Fig. 4). The eddy kinetic energy does not peak as high in the lower-shear case as in the barotropic case, but it levels off at about the same value as in the barotropic-shear case by day 20. The differences between barotropic- and lower-shear anomalies are explored further in Fig. 5. For barotropic-shear anomalies the transition from anticyclonic to cy-

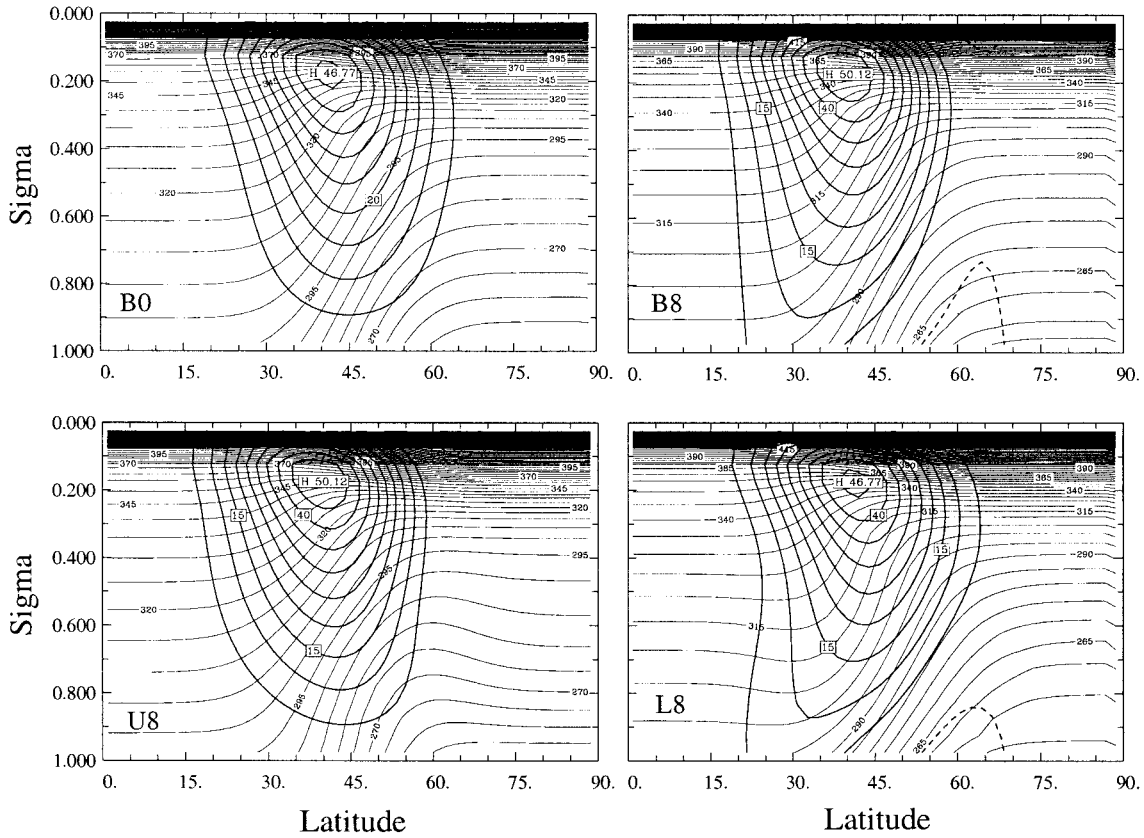


FIG. 3. Latitude vs sigma cross sections of initial zonal wind and potential temperature for cases B0, B8, U8, and L8. Contour intervals are 5 m s^{-1} and 5 K . The 305-K contour crosses the equator at about $\sigma = 0.8$.

clonic behavior occurs between anomalies of 7 and 8 m s^{-1} . The B8 case is anomalously persistent. Cases with stronger initial shears (9 and 10 m s^{-1}) experience a drop in eddy energy that is associated with eddy absorption on the poleward flank of the jet and equator-

ward movement of the jet. These cases still retain eddy energy for a longer time than do subcritical cases. If the shear is applied only in the lower troposphere (Fig. 5b), then the transition occurs a little earlier, and $\sim 7 \text{ m s}^{-1}$ is the critical shear to produce minimum acceleration and maximum eddy persistence, but other features are similar. Thus, cyclonic shear decreasing in amplitude with height is slightly more effective in inducing cyclonic behavior than is barotropic shear.

One may question whether the barotropic-shear anomaly or the baroclinic-shear anomaly causes the difference between the L and U cases. To address this concern we compare some hybrid cases in Fig. 6. This figure shows the sharp contrast between B6 and B8. As the barotropic shear is increased from 6 to 8 m s^{-1} , the eddy life cycle transitions from rapid decay to a long-lived undular wave as described in THM and HZ. If we begin with B6 and add a 2 m s^{-1} shear with the lower (B6 + L2) or upper (B6 + U2) structures, we see that the B6 + L2 case is almost identical to the B8 case, but the eddy energy of the B6 + U2 case decays only a little more slowly than the B6 case. This comparison suggests that the lower-level meridional shear is much more important than the upper-level shear in determining wave life cycle behavior. Since the baroclinic shear

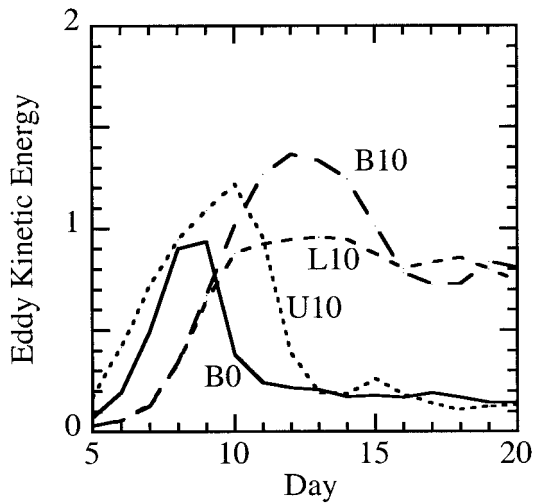


FIG. 4. Hemispheric eddy kinetic energy as a function of time for life cycle cases B0, B10, L10, and U10.

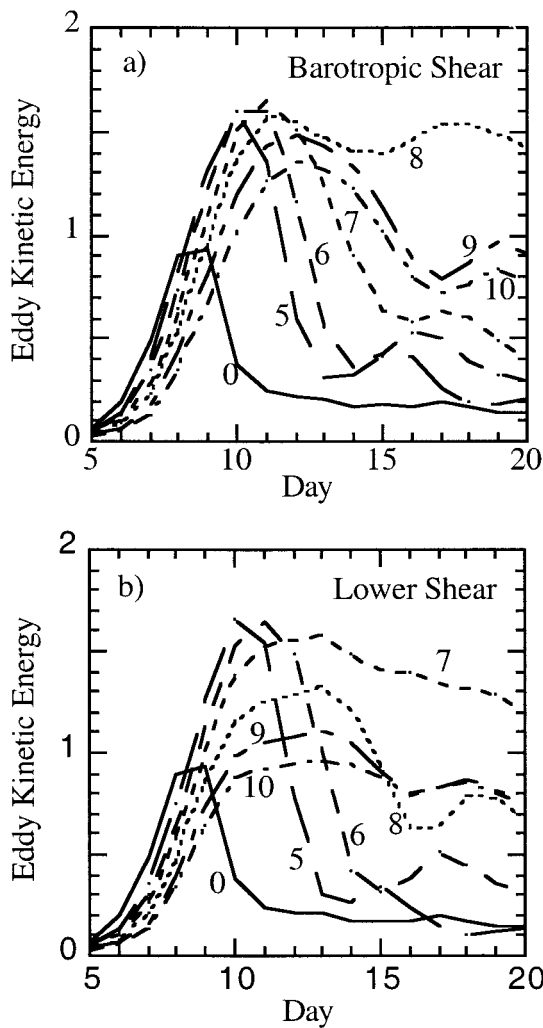


FIG. 5. Same as Fig. 4, except for (a) barotropic shear with $U_0 = 0, 5, 6, 7, 8, 9,$ and 10 m s^{-1} and (b) lower shear with the same values of U_0 .

associated with the 2 m s^{-1} anomalies is small, and the effect of the addition is large and equivalent to a barotropic anomaly, we believe that it is the meridional shear crossing a threshold that is the critical difference, rather than a small change in baroclinicity of the zonal flow. It is clear that this critical threshold is associated with the low-level winds, rather than with the upper-tropospheric winds. Although the baroclinic shear does introduce potential vorticity (PV) anomalies near the jet core, their magnitude is small and, we believe, relatively unimportant. Quasi-barotropic advective processes that set the shape of the wave at low levels determine the differences in life cycle evolution.

To assess the possible influence of baroclinic-shear anomalies on the life cycle behavior, we consider differences in eddy fluxes between the B8 and B6 + L2 cases by comparing each of them to the B6 case. Figure 7 shows the difference of the eddy fluxes of heat, mo-

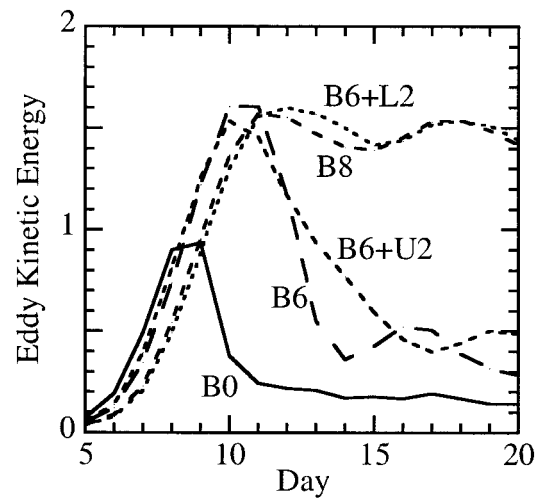


FIG. 6. Same as Fig. 4, but for life cycle cases B0, B6, B8, B6 + L2, and B6 + U2.

mentum, and potential vorticity between cases B6 + L2 and B6 plus the difference in eddy potential vorticity flux between cases B8 and B6. In every case the anticyclonic case (B6) has much larger eddy fluxes. The change in eddy heat flux is only large at upper levels, and it is associated with the large difference in PV fluxes there. The momentum flux change is very large in a relative sense, with the peak value in the cyclonic case ($32 \text{ m}^2 \text{ s}^{-2}$) less than half of the peak value in the anticyclonic case ($75 \text{ m}^2 \text{ s}^{-2}$). The important point here is that the eddy fluxes averaged over the 20-day life cycle are virtually identical in the B6 + L2 and B8 cases, suggesting either that the baroclinic and barotropic effects of the upper-level wind changes cancel exactly, or that both are unimportant. It is interesting that zonal flow changes at low levels introduce changes in eddy structure that are reflected in eddy fluxes at upper levels. The anomalies in induced eddy fluxes are not located where the critical zonal wind perturbations are applied. We have done a variety of other experiments to investigate the importance of upper-level shears and the baroclinic anomalies and have found little evidence to suggest that they are important. For example, the case B8 + U2 is virtually identical to B8. We will see next that the identity of the eddy fluxes leads naturally to virtual identity of the zonal flow accelerations produced.

4. Zonal flow accelerations

The zonal flow accelerations produced during the eddy life cycle are related to the eddy flux and eddy kinetic energy changes and so are also very sensitive to the initial barotropic shear. The net change in zonal mean wind over the 20-day experiments is most sensitive to the initial meridional shear near the surface, as shown in Fig. 8. As discussed by HZ, in the basic case the jet moves poleward with maximum westerly

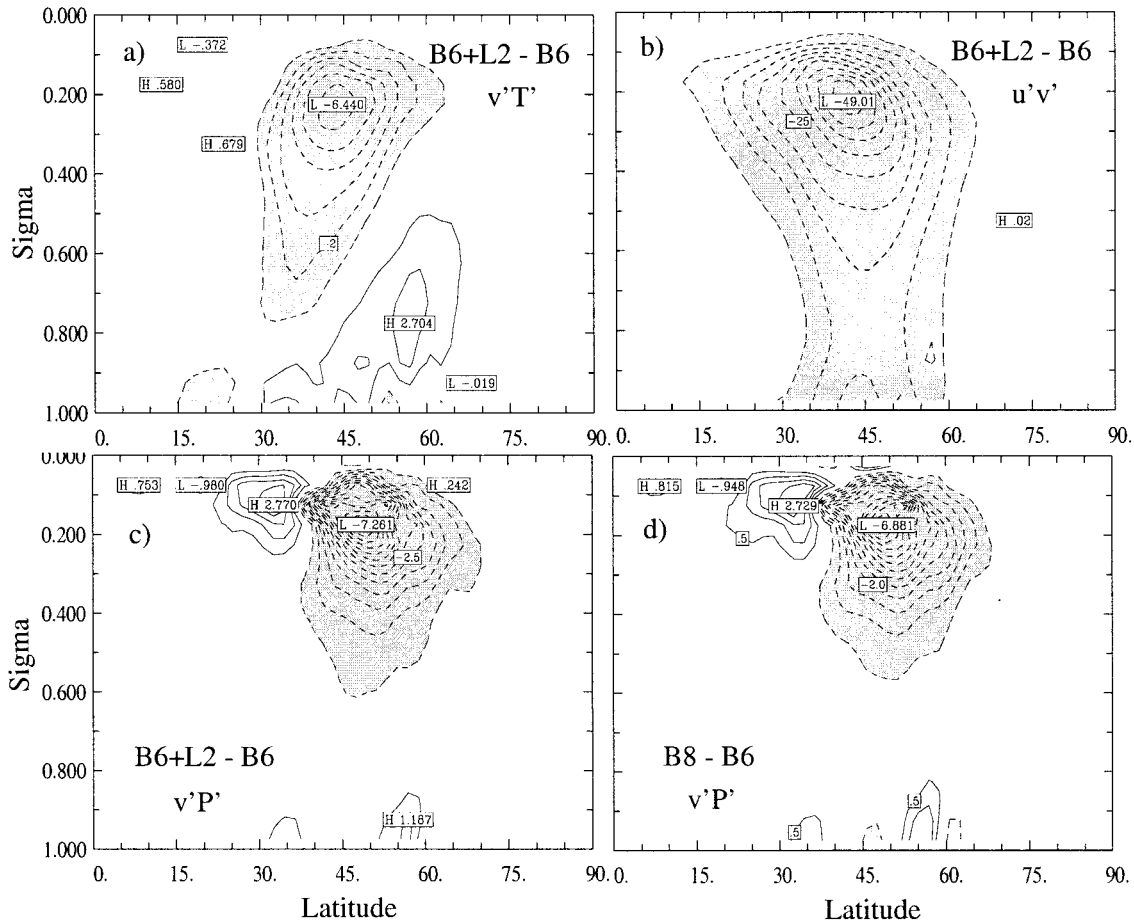


FIG. 7. Latitude vs sigma cross sections of differences between cyclonic and anticyclonic cases of life cycle-averaged eddy fluxes; (a) eddy heat flux [contour interval (c.i.) = 2 K m s^{-1}], (b) eddy momentum flux (c.i. = $5 \text{ m}^2 \text{ s}^{-2}$), (c) eddy potential vorticity flux for case B6 + L2 minus case B6, and (d) eddy potential vorticity flux for B8 minus B6 (c.i. = 0.5 PVU m s^{-1} , where $1 \text{ PVU} = 10^{-6} \text{ m}^2 \text{ s}^{-1} \text{ K kg}^{-1}$).

accelerations near 53° , while strong easterly accelerations are produced equatorward near 30° . In the case with strong initial cyclonic barotropic shear, B10, the westerly wind is accelerated equatorward of the initial jet core near 40° and easterlies are produced poleward near 60° . The wave life cycle accentuates the initial cyclonic shear anomaly and the jet moves equatorward, if the initial zonal mean cyclonic rotation about the mean jet is strong enough. The net acceleration produced in case U10 is very similar to that produced in the basic experiment B0; both produce poleward movement and anticyclonic shear around the latitude of the initial baroclinic jet. In contrast, the total acceleration in case L10 is virtually identical to that produced by case B10; both produce equatorward movement and cyclonic shear of the zonal jet. This again suggests that the initial meridional shear in the lower troposphere determines the magnitude and shape of the zonal flow accelerations, and that the upper-level shear has only a minor effect.

Again we can use the sharp transition in behavior

between cases B6 and B8 to minimize the possible influence of baroclinic-shear anomalies. The zonal wind accelerations for cases B6, B8, B6 + U2, and B6 + L2 are shown in Fig. 9. Case B6 is similar to B0 in that strong poleward jet movement and anticyclonic-shear development are produced. Case B8 is near the point where the eddy kinetic energy is most long-lived and the zonal flow accelerations are weakest. For stronger initial cyclonic shears (e.g., B10 in Fig. 8) the eddy energy is not quite as well preserved and fairly strong cyclonic accelerations are produced. As the initial cyclonic shear is increased above 8 m s^{-1} , poleward wave breaking is enhanced and stronger cyclonic shear accelerations are produced. As was the case with the eddy kinetic energy evolution, the zonal flow accelerations produced in the B6 + L2 case are virtually identical to those in case B8, while the accelerations for case B6 + U2 are indistinguishable from case B6. This again suggests the overwhelming importance of low levels in determining life cycle behavior at all levels.

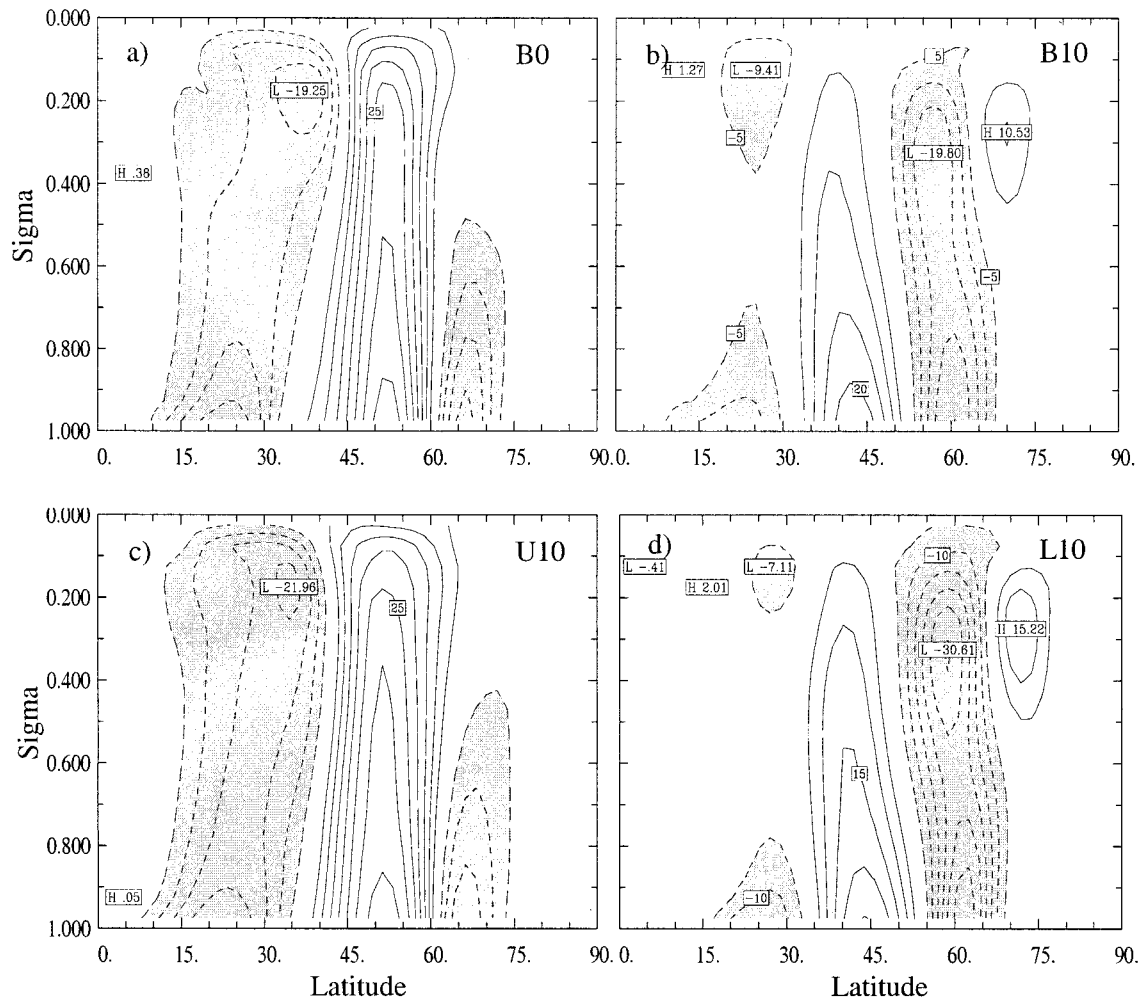


FIG. 8. Latitude vs sigma cross sections of the zonal wind on day 20 minus the zonal wind on day 0 for life cycle cases B0, B10, U10, and L10. Contour interval is 5 m s^{-1} , and values less than -5 m s^{-1} are shaded. Zero contour is not plotted.

5. Eddy structure

We now show some differences in eddy structure that are produced by barotropic shears at low levels. We begin by comparing the evolution of PV and winds on the 305-K theta surface. We choose the 305-K surface because in the initial cross sections (Fig. 3) it extends from the lower stratosphere poleward of the jet, drops steeply in altitude across the jet, and extends into the lower troposphere on the equatorward side of the jet. At 50° the 305-K surface is at a pressure of 300 hPa, but at 30° it is down to 800 hPa. This level is thus likely to capture the structure of high-PV anomalies that extend downward and influence surface features. It will also show the early nonlinearity of the life cycle much more clearly than PV charts at higher levels, where strong zonal mean PV gradients dominate the picture.

The PV evolutions on the 305-K surface for the B6, B6 + L2, and B8 cases between days 6 and 12 are shown in Fig. 10. The PV evolution of the B6 + L2 case is nearly identical to that of the B8 case, as is its

eddy kinetic energy and zonal wind evolution. The B6 case is different in that it develops the greater meridional elongation of the cyclone that leads to narrowing of the cyclone and to a southwest–northeast tilt that eventually leads to eddy breakdown and strong poleward momentum flux. The narrowing and westward tilt of the nose of the PV maximum in the B6 case is associated with stronger anticyclonic circulations on either side of the cyclone. It is useful to consider the effect of these two anticyclones on the high-PV cyclone between them in order to understand the wave breakdown. Think of the wind anomalies associated with the two anticyclonic vortices and the influence of these wind anomalies on the advection of a cyclonic vorticity anomaly between them. The strength of the anticyclonic wind anomalies decreases with distance from the center of the anticyclone. The anticyclone to the east of the cyclone narrows the cyclone by inducing poleward flow of high-PV air on the eastern side of the cyclone. The anticyclone to the west induces equatorward extension of the PV max-

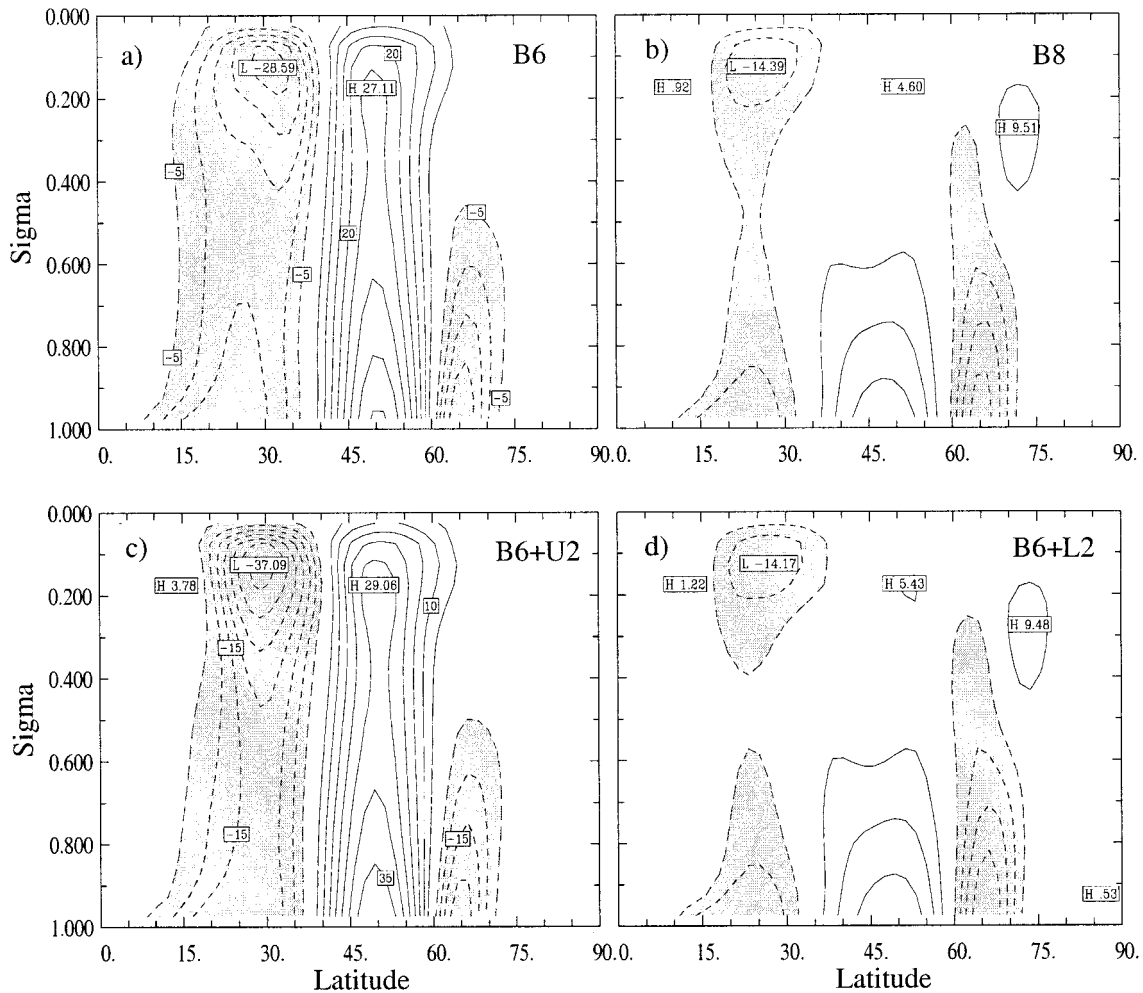


FIG. 9. Same as Fig. 8, except for cases B6, B8, B6 + U2, and B6 + L2.

imum and wrapping of high-PV filaments in a southwest direction around the anticyclone, because it induces equatorward advection on the western side of the cyclone. The two anticyclones on either side can thus be imagined to produce the thinning and southwest–northeast tilt of the cyclone.

Turn now to a consideration of the evolution of the high potential vorticity tongue associated with the cyclone. In each case shown in Fig. 10 a narrow tongue of high-PV air extends equatorward and then curls downwind and back poleward to form a broad cyclone. The curling back of the high-PV air is most evident in the hook structure seen on day 8. In the cases of cyclonic evolution (B8 and B6 + L2) the tongue curls downstream a little farther to the east and incorporates more low-PV air, so that the resulting cyclone is broader in the zonal direction. The downstream ridging is weaker than in the anticyclonic case, as can be seen in the weaker poleward advection of low-PV air to the east of the low. A critical difference is that, in the cases of cyclonic evolution, easterlies wrap around the poleward

side of the cyclone, making it a closed circulation, cut off from the stratospheric reservoir of high-PV air. This closed, almost isotropic, cyclonic vortex is very stable, as can be seen most clearly on day 12. After day 12 the B6 case continues to break down into a zonal flow, whereas both cases B8 and B6 + L2 remain undular with high values of eddy energy.

The main change that occurs as the initial shear is increased is that the equatorward extension and the narrowness of the lobe of high-PV air decreases with increasing cyclonic rotation of the initial wind. With more cyclonic rotation of the initial wind, the high-PV center becomes more isotropic by becoming zonally elongated and meridionally constrained. Also, because of more mixing of low-PV air into the cyclone, the maximum PV values in the cyclone decrease with increasing cyclonic rotation of the initial zonal wind.

The important structural differences can also be seen in the surface pressure and wind fields, and differences in the strength of the anticyclone are apparent at a very early stage. Whitaker and Snyder (1993) and Balasu-

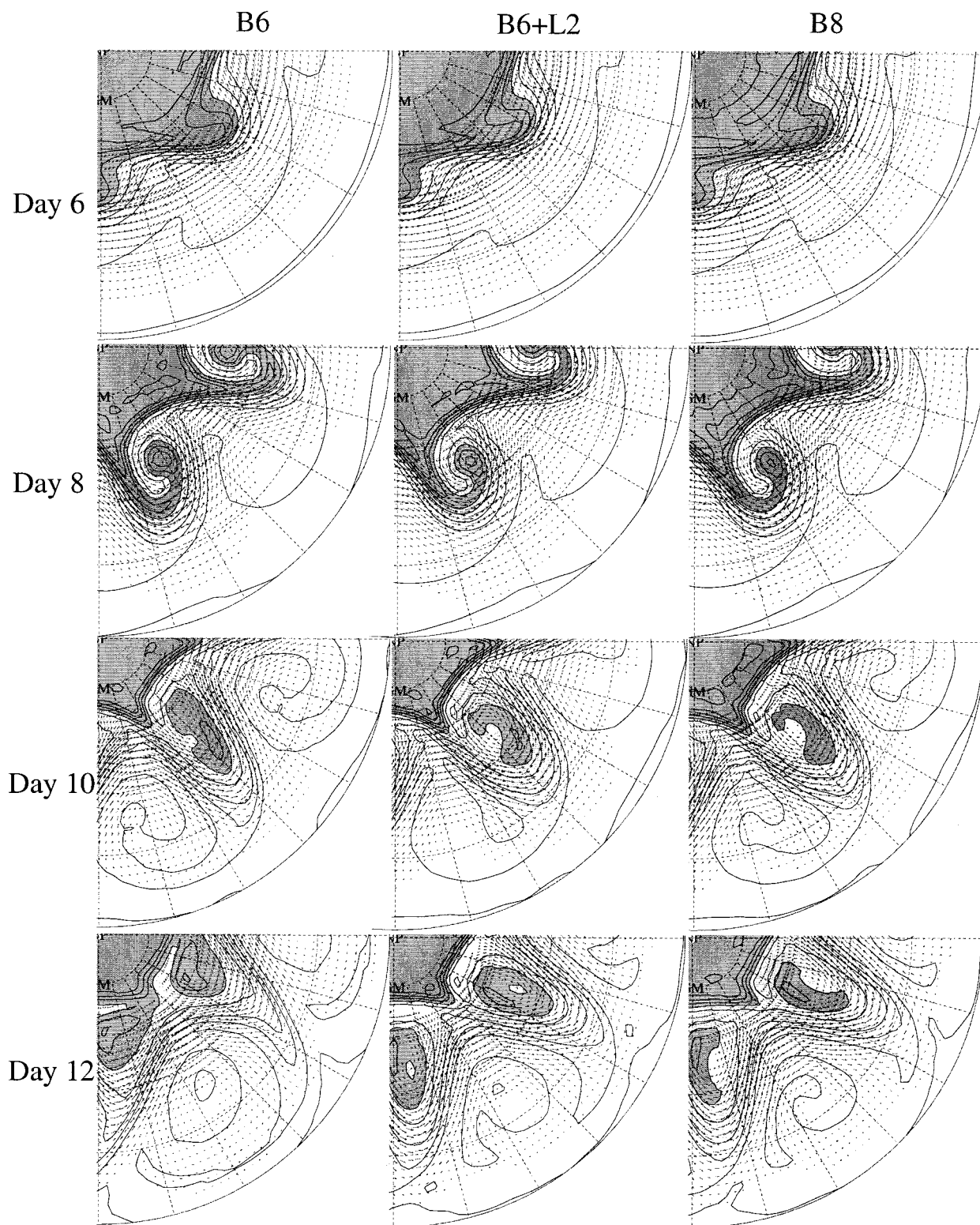


FIG. 10. Maps of potential vorticity and wind vectors on the 305-K potential temperature surface for days 8–12 of experiments B6, B6 + L2, and B8. Here, PV values greater than 1 PVU are lightly shaded and values greater than 2 PVU are darkly shaded.

bramanian and Garner (1997) particularly emphasized the role of the low-level anticyclone. Figure 11 shows the surface pressure and wind fields for the same cases and times as in Fig. 10. At day 6 and even earlier (not shown) a significant difference in the strength of the anticyclone is evident. At this time the differences in the PV field at 305 K are subtle, and at higher levels the PV fields look very similar indeed. So we can see a signature of the difference between the anticyclonic and cyclonic cases very early in the experiment if we look at the surface map. At low levels the small-shear anomaly is important, and the flow is nonlinear at the early stages. As the flow evolves, the difference in the intensity of the highs persists, and by day 10 the surface low begins to elongate in the north–south direction and the low center begins to be pushed poleward. By day 12 the process of eddy breakdown and “zonalization” of the pressure field is well under way, with the low displaced farther poleward and the anticyclones also beginning to merge together to form a zonal high pressure belt. In the cyclonic case the low pressure centers retain their strength and latitude and the highs persist as wave-like features.

6. Normal mode calculations

Since the differences in structure appear at early stages at low levels, it is interesting to compute the changes in unstable normal-mode structure induced by shear. Balasubramanian and Garner (1997) showed that eddy momentum fluxes associated with normal modes are sensitive to meridional shear. We show here that it is the meridional shear at low levels that is important in producing these differences. We have analyzed the normal modes of all the initial wind profiles studied here. These calculations were done at T42L20 resolution. To illustrate the differences in normal-mode structure, we show the zonal wind profiles, normalized eddy kinetic energy, normalized eddy heat flux, and normalized eddy momentum flux in Fig. 12. Wave amplitude is normalized by setting hemispherically integrated eddy energy equal to that of a wind speed perturbation of 1 m s^{-1} at all levels and latitudes. We show only three representative cases: B0, L8, and U10. The eddy momentum fluxes for case L8 are very different from those of case B0 at all levels. The cyclonic shear at low levels induces stronger equatorward momentum fluxes at all levels, suggesting that the momentum flux at all levels is sensitive to low-level shear. Case B8 (not shown) is very similar to case L8 at all levels, indicating again that the normal mode eddy momentum fluxes at upper levels are determined by the wind profile at low levels, not by the local wind at upper levels. The eddy fluxes for the U10 wind profile, on the other hand, are very similar to those for B0. The cyclonic rotation at upper levels has little effect on the momentum fluxes there.

The normal-mode calculations are not sufficient to predict the transition from anticyclonic to cyclonic life

cycle behavior. The eddy fluxes are not significantly different for cases B6 and B8, for example. While linear modes respond linearly to small changes in shear, the rapid transition in life cycle behavior and ending state occurs precipitously across a narrow range of shear parameter. The mechanisms producing this transition in life cycle behavior must be fundamentally nonlinear.

7. Discussion and conclusions

We have shown that the influence of the meridional shear of the initial zonal mean wind on eddy life cycles is mostly dependent on the wind shear near the surface. Upper-level shear plays a very secondary role in determining both the fate of eddy kinetic energy in the latter stages of the life cycle and the associated zonal flow accelerations. Sufficiently strong cyclonic rotation of the zonal wind near the surface can induce cyclonic accelerations at all levels, while unsheared or anticyclonically sheared zonal flows tend to produce anticyclonic accelerations relative to the latitude of the original baroclinic jet. The simplest explanation for the dominance of low-level shears seems to be that the steering level, where the wind speed is near the phase speed for the disturbances of interest, occurs in the lower troposphere. It is near this level that advection determines the shape of the wave. The shape of the wave at low levels determines the structure and magnitude of the eddy potential vorticity flux at upper levels. The eddy fluxes at upper levels are a diagnostic of strong wave–mean flow interactions, but the critical flow conditions that determine those fluxes occur at lower levels. A fundamental argument is that the levels where the phase speed of the wave and the wind speed are equal are the levels where meridional-shear variations are most important. One can also simply note that the winds are weak near the surface and stronger aloft, so that a wind speed change of fixed magnitude will always be more important at lower levels, where the winds are weaker.

In previous papers we have argued that the strong positive feedback between meridional shear of the barotropic component of the mean wind and the eddies that grow on that mean wind structure can form the fundamental explanation for the dominant mode of low-frequency variability in the Southern Hemisphere (Yu and Hartmann 1993; Hartmann 1995; Hartmann and Lo 1998; HZ). Similar dynamics may form an explanation for nearly zonally symmetric variations in the Northern Hemisphere. Although eddy life cycles tend to force large barotropic accelerations of zonal flow, surface drag will tend to damp surface zonal flow anomalies more quickly than upper-level anomalies. Robinson (1996) showed in a two-level model that the zonal flow vacillation occurs only in the presence of “strong” drag but that the persistence of eddy flux anomalies is dependent on the presence of barotropic zonal flow anomalies. Surface drag is necessary to overcome the stabilization resulting from both the baroclinic and baro-

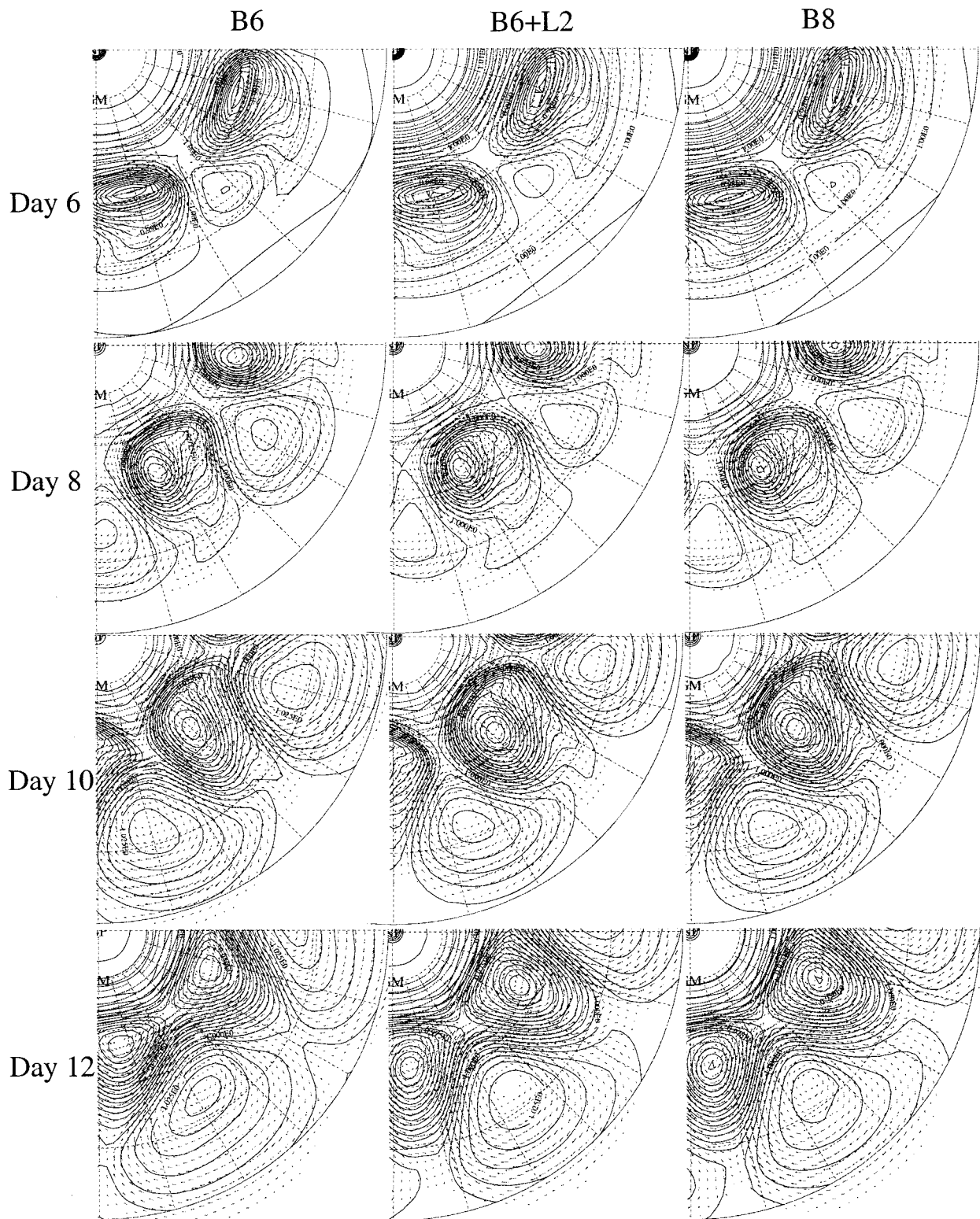


FIG. 11. Maps of surface pressure and surface wind for the same cases and times as in Fig. 10.

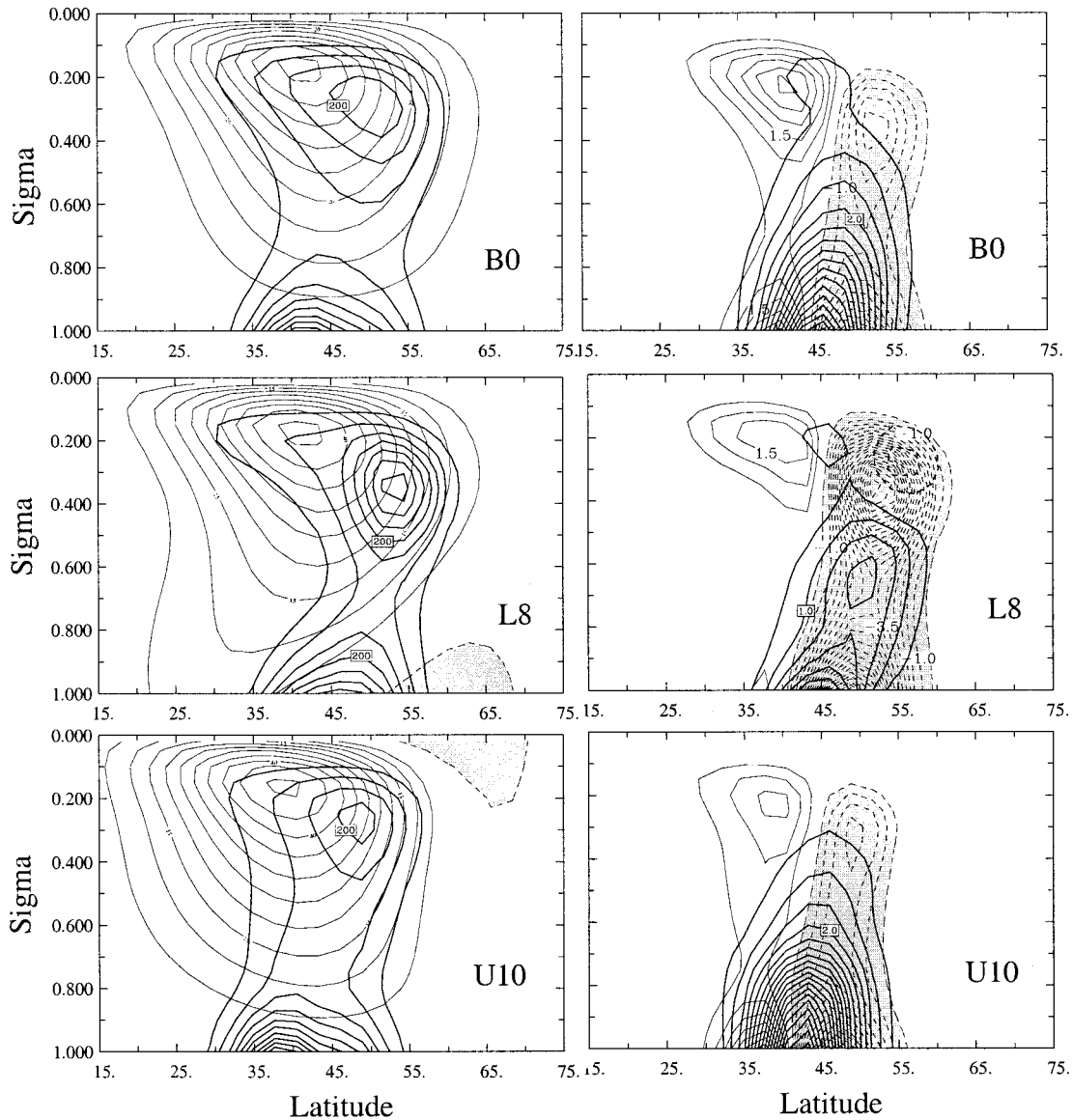


FIG. 12. Latitude–sigma cross sections of normal-mode structure for cases B0, L8, and U10. Zonal wind and normalized eddy kinetic energy are shown on the left. Zonal wind values less than -5 m s^{-1} are shaded. Normalized eddy heat flux (heavier lines) and eddy momentum flux (values less than -0.5 shaded) are shown on the right.

tropic zonal wind shear changes produced by eddy life cycles. It presumably achieves this both by reducing the barotropic shears and by increasing the baroclinic shear, and so making the next cycle of baroclinic growth possible. On the other hand, it seems possible that if surface drag were too strong, it would reduce zonal flow vacillation by suppressing both surface zonal flow anomalies and the intensity of the eddies growing on that zonal flow.

According to the results presented here, zonal flow shear anomalies near the surface have the largest influence on the eddy life cycles and resulting zonal flow accelerations, while upper-level winds are of less importance. The relatively weak surface friction over the

oceans may be ideal for strong eddy-driven zonal flow vacillation. It is certainly true that zonal flow vacillation is of largest magnitude over the oceans both in the Southern Hemisphere and in the Northern Hemisphere (e.g., Thompson and Wallace 1998). Of course eddy-driven vacillation can occur only in storm tracks where eddies are active, and these tend to occur at longitudes determined by topography and surface heating gradients rather than by friction, which are coincidentally over the oceans. Numerical experiments can test the idea that eddy-driven zonal flow vacillation is favored by surface friction corresponding to values over the ocean.

Acknowledgments. This work was supported by the

Climate Dynamics Program of the Atmospheric Sciences Division of the National Science Foundation under Grants ATM-9313383 and ATM-9873691. The author is grateful to Drs. I. M. Held and P. J. Kushner for providing one of the model codes used in this investigation. Dr. J.-Y. Yu and Mr. P. Zuercher helped develop the model and analysis codes while they were students at UW. Mr. M. L. Michelsen gave advice on computational and graphical problems and efficiently parallelized the finite element code. Three anonymous reviewers gave very useful suggestions.

REFERENCES

- Balasubramanian, G., and S. T. Garner, 1997: The role of momentum fluxes in shaping the life cycle of a baroclinic wave. *J. Atmos. Sci.*, **54**, 510–533.
- Bretherton, F. P., 1966: Critical layer instability in baroclinic flows. *Quart. J. Roy. Meteor. Soc.*, **92**, 325–334.
- Buizza, R., and T. N. Palmer, 1995: The singular-vector structure of the atmospheric global circulation. *J. Atmos. Sci.*, **52**, 1434–1456.
- Bush, A. B. G., and W. R. Peltier, 1994: Tropopause folds and synoptic-scale baroclinic wave life cycles. *J. Atmos. Sci.*, **51**, 1581–1604.
- Davies, H. C., C. Schär, and H. Wernli, 1991: The palette of fronts and cyclones within a baroclinic wave development. *J. Atmos. Sci.*, **48**, 1666–1689.
- Edmon, H. J., B. J. Hoskins, and M. E. McIntyre, 1980: Eliassen–Palm cross sections for the troposphere. *J. Atmos. Sci.*, **37**, 2600–2616; Corrigendum, **38**, 1115.
- Gall, R. L., 1976: Structural change of growing baroclinic waves. *J. Atmos. Sci.*, **33**, 374–390.
- Hartmann, D. L., 1995: A PV view of zonal flow vacillation. *J. Atmos. Sci.*, **52**, 2561–2576.
- , and F. Lo, 1998: Wave-driven zonal flow vacillation in the Southern Hemisphere. *J. Atmos. Sci.*, **55**, 1303–1315.
- , and P. Zuercher, 1998: Response of baroclinic life cycles to barotropic shear. *J. Atmos. Sci.*, **55**, 297–313.
- , R. Buizza, and T. N. Palmer, 1995: Singular vectors: The effect of spatial scale on linear growth of disturbances. *J. Atmos. Sci.*, **52**, 3885–3894.
- Heckley, W. A., and B. J. Hoskins, 1982: Baroclinic waves and frontogenesis in a non-uniform potential vorticity semi-geostrophic model. *J. Atmos. Sci.*, **39**, 1999–2016.
- Held, I. M., and M. J. Suarez, 1994: A proposal for the intercomparison of the dynamical cores of atmospheric general circulation models. *Bull. Amer. Meteor. Soc.*, **75**, 1825–1830.
- James, I. N., 1987: Suppression of baroclinic instability in horizontally sheared flows. *J. Atmos. Sci.*, **44**, 3710–3720.
- Nakamura, N., 1993: Momentum flux, flow symmetry, and the nonlinear barotropic governor. *J. Atmos. Sci.*, **50**, 2159–2179.
- Robinson, W. A., 1996: Does eddy feedback sustain variability in the zonal index? *J. Atmos. Sci.*, **53**, 3556–3569.
- Rotunno, R., W. C. Skamarock, and C. Snyder, 1998: Effects of surface drag on fronts within numerically simulated baroclinic waves. *J. Atmos. Sci.*, **55**, 2119–2129.
- Simmons, A. J., and B. J. Hoskins, 1978: The life cycles of some nonlinear baroclinic waves. *J. Atmos. Sci.*, **35**, 414–432.
- , and —, 1980: Barotropic influences on the growth and decay of nonlinear baroclinic waves. *J. Atmos. Sci.*, **37**, 1679–1684.
- Thompson, D. W. J., and J. M. Wallace, 1998: The Arctic oscillation signature in the wintertime geopotential height and temperature fields. *Geophys. Res. Lett.*, **25**, 1297–1300.
- Thorncroft, C. D., and B. J. Hoskins, 1990: Frontal cyclogenesis. *J. Atmos. Sci.*, **47**, 2317–2336.
- , —, and M. E. McIntyre, 1993: Two paradigms of baroclinic-wave life-cycle behaviour. *Quart. J. Roy. Meteor. Soc.*, **119**, 17–55.
- Wernli, H., R. Fehlmann, and D. Lüthi, 1998: The effect of barotropic shear on upper-level induced cyclogenesis: Semigeostrophic and primitive equation numerical simulations. *J. Atmos. Sci.*, **55**, 2080–2094.
- Whitaker, J. S., and C. Snyder, 1993: The effects of spherical geometry on the evolution of baroclinic waves. *J. Atmos. Sci.*, **50**, 597–612.
- Yu, J.-Y., and D. L. Hartmann, 1993: Zonal flow vacillation and eddy forcing in a simple GCM of the atmosphere. *J. Atmos. Sci.*, **50**, 3244–3259.